catalysts

MDPI

Article

CO_2-Induced Fibrous Zn Catalyst Promotes Electrochemical Reduction of CO_2 to CO

Mengquan Guo [1], Xiangxiang Li [1], Yuxin Huang [1], Linfa Li [1], Jixiao Li [1], Yiren Lu [1], Yanhong Xu [2,*] and Lihong Zhang [1,*]

[1] Department of Catalysis Science and Technology and Tianjin Key Laboratory of Applied Catalysis Science & Technology, School of Chemical Engineering and Technology, Tianjin University, Tianjin 300350, China; gmq_0105@tju.edu.cn (M.G.); lixx_37@tju.edu.cn (X.L.); youningtdzhy@163.com (Y.H.); lithium@tju.edu.cn (L.L.); tokinobug@163.com (J.L.); luyiren@tju.edu.cn (Y.L.)

[2] Department of Materials Engineering, Xuzhou College of Industrial Technology, Xuzhou 221140, China

* Correspondence: xuyanh@mail.xzcit.cn (Y.X.); zlh_224@tju.edu.cn (L.Z.); Tel.: +86-150-6212-8662 (Y.X.); +86-150-2225-5828 (L.Z.)

Abstract: The electrochemical reduction of CO_2 is a promising strategy to achieve efficient conversion and utilization. In this paper, a series of Zn catalysts were prepared by electrodeposition in different atmospheric conditions (N_2, CO_2, H_2, CO). A fibrous Zn catalyst (Zn-CO_2) exhibits high electrochemical activity and stability. The Zn-CO_2 catalyst shows 73.0% faradaic efficiency of CO at −1.2 V vs. RHE and the selectivity of CO almost did not change over 6 h in −1.2 V vs. RHE. The excellent selectivity and stability is attributed to the novel fibrous morphology, which increases the electrochemical active surface area. X-ray diffraction (XRD) results show that Zn-CO_2 catalyst has a higher proportion of Zn (101) crystal planes, which is considered to be conducive to the production of CO. The search further demonstrates the importance of morphology control for the preparation of highly active and stable catalysts.

Keywords: electrocatalysis; electrodeposition; CO_2 reduction; fibrous structure; porous

Citation: Guo, M.; Li, X.; Huang, Y.; Li, L.; Li, J.; Lu, Y.; Xu, Y.; Zhang, L. CO_2-Induced Fibrous Zn Catalyst Promotes Electrochemical Reduction of CO_2 to CO. *Catalysts* **2021**, *11*, 477. https://doi.org/10.3390/catal11040477

Academic Editor: Ali Seifitokaldani

Received: 18 March 2021
Accepted: 5 April 2021
Published: 8 April 2021

1. Introduction

Over the past few years, heavy consumption of fossil fuels has increased the concentration of carbon dioxide (CO_2) in the atmosphere, leading to many environmental problems such as greenhouse effect and energy dilemma [1]. It is widely accepted that reducing the concentration of CO_2 is a key to solving environmental problems. The transformation and utilization of CO_2 has become the focus of research for researchers. [2]. CO_2 can be converted to high-value products such as carbon monoxide, methane, formic acid, methyl alcohol, ethyl alcohol, ethylene and so on [3–8], by electrochemical CO_2 reduction reaction (CO_2RR) under mild conditions. Therefore, electrochemical CO_2RR is the most promising technology to achieve the conversion and utilization of CO_2. The challenge of electrochemical CO_2RR is the preparation of catalysts with high activity, selectivity and stability, which is the core for catalytic research.

Up to now, researchers have developed a number of catalysts for CO_2RR. Noble metals such as Au [9–13] and Ag [14–19] are known to be the best metal catalysts for converting CO_2 to CO with high activity and selectivity. However, it is difficult to use in large quantities in industrialization, due to the high price and scarce reserve of precious metals. Therefore, research into efficient non-noble metal catalysts has become an important part of the industrial application of electroreduction of CO_2. Zn, an abundant metal, is proved to be an outstanding electrocatalyst to produce CO [20–23]. However, there are many challenges for the practical application of CO_2 reduction. The reaction still suffers from poor stability and faradaic efficiency (FE) of the primary product. Therefore, the preparation of catalysts with high activity and selectivity is the core of future development.

There are many researchers who have studied Zn catalyst in recent years. In order to improve the performance of Zn catalysts for CO_2RR, many strategies have been used in the preparation of catalysts, such as electrodeposition, anodization, oxide reduction [24]. Preparation of Zn catalyst with large surface area is considered as an effective method to enhance the activity of the catalyst. For example, electrodeposited Zn dendrite electrode has a surface area of around 90 cm^2/cm^2_{Geo}, corresponding to over 80 times higher surface area than Zn bulk foil electrodes, and the FE of CO (FE_{CO}) is around 3-fold higher [25]. Recently, some researchers have studied the synthesis of catalysts in aqueous electrolyte with CO_2-rich condition to improve the activity of catalysts. For example, Wang et al. synthesized Pb catalyst in an aqueous electrolyte with CO_2-rich condition, and formic acid FE reached 90.5% [26]. Wang et al. reported Cu catalyst, which was synthesized under CO_2 reduction conditions, with a 90% FE for C_{2+} [27]. This indicates that CO_2 plays a key role in the preparation of highly active catalysts by electrodeposition.

In this work, a series of Zn catalysts were prepared by electrodeposition in different gas-saturated (N_2, CO_2, H_2, CO) $Zn(NO_3)_2$ aqueous solutions. Linear sweep voltammetry (LSV), cyclic voltammetry (CV) and Tafel slope were employed to study the performances of different Zn catalysts for CO_2RR. Zn-CO_2 catalysts have the best activity and selectivity for electrochemical CO_2RR. The Zn-CO_2 electrode shows 73.0% faradaic efficiency of CO at −1.2 V vs. RHE. The partial current density of CO is 6.1 mA/cm^2 and the selectivity of CO has almost not changed over 6 h in −1.2 V vs. RHE. X-ray diffraction (XRD), scanning electron microscopy (SEM), transmission electron microscopy (TEM) and X-ray photoelectron spectroscopy (XPS) characterization methods were used to investigate the relation of the structure and excellent activity of as-prepared catalysts in detail. XRD results show that Zn-CO_2 catalyst has a higher proportion of Zn (101) crystal planes. The SEM images show that the surface of Zn-CO_2 catalyst is covered by porous fibers with uniform tiny pores, which increases the electrochemical active surface area (ECSA). This is the main reason for the excellent catalytic performance of Zn-CO_2 catalysts. The research prepared a Zn catalyst with new morphology and excellent activity and stability of electrochemical CO_2RR, which develops a new means and idea for the preparation of more efficient and stable Zn catalysts. This work is of great value and significance in solving the challenge of low activity and poor stability in electrochemical CO_2RR.

2. Results and Discussion

2.1. Electrochemical Performance

The electrochemical performance of the prepared electrodes for CO_2RR was evaluated by linear sweep voltammetry (LSV) at 5 mV/s in pure $KHCO_3$ electrolyte solution saturated with CO_2. As shown in Figure 1a, the current density of the Zn-CO_2 electrode is the highest and far higher than that of other electrodes, which indicates that the Zn-CO_2 electrode has the best catalytic activity. To evaluate the electrochemical activity of Zn catalysts, the controlled potential electrolysis experiment was conducted at different cathodic potential to the CO_2-saturated $KHCO_3$ electrolyte. Before the controlled potential electrolysis experiment, cyclic voltammetry (CV) was performed over the potential range from −0.55 V vs. RHE to −1.35 V vs. RHE (50 mV/s) for 20 cycles to reduce the oxide layer of the catalyst. The main gas products which were detected every 30 min by gas chromatography (GC) were CO and H_2. Figure 1b shows that the FE_{CO} for Zn foil electrode gradually increases with the decrease of applied voltage, and reaches a maximum of 47.0% at −1.3 V. Zn-N_2 electrode has a FE_{CO} at 66.2% at −1.0 V vs. RHE, and decreases gradually with the decrease of applied voltage which indicates that the H_2 evolution reaction (HER) is more serious at more negative voltage for Zn-N_2 electrode. This can also be demonstrated by the diagram of the FE of H_2 as a function of voltage (Figure 1c), which FE_{H2} increases gradually when the voltage exceeds −1.2 V vs. RHE. The maximal FE_{CO} is found on Zn-CO_2 electrode with 73.0% at −1.2 V vs. RHE (Figure 1b), and with the lowest FE_{H2} of 32.6% (Figure 1c), and the partial current density of CO is 6.1 mA/cm^2 at −1.2 V vs. RHE (see Table S1). This indicates the production of CO is promoted and the production

of H_2 is inhibited at −1.2 V. The Zn-H_2 electrode has a FE_{CO} of 47.9% at −1.2 V vs. RHE, and the Zn-CO electrode has a FE_{CO} at 56.7% at −1.1 V vs. RHE. These results show that the catalyst prepared by electrodeposition in CO_2-saturated $Zn(NO_3)_2$ aqueous solution can effectively promote the production of CO. To evaluate the long-term performance of the Zn-CO_2 electrode, a chronoamperometry experiment at −1.2 V vs. RHE was carried out. As shown in Figure 1d, the current density is stable at 4.6 mA/cm^2, and the FE_{CO} remains unchanged (~73.0%) over 6 h. The stability evaluations of other electrodes under the same conditions were also carried out, and the results are shown in Figure S1. The FE_{CO} for Zn foil and Zn-H_2 electrode decreased gradually with the increase of time during 6 h, while their current density is still stable. The current density for the Zn-N_2 electrode maintains stable before 5 h and then decreases dramatically after reaction of 5 h, at the same time, the FE_{CO} fluctuates between 40.0% and 60.0%. A similar phenomenon appears in the Zn-H_2 electrode. This shows the Zn foil, Zn-N_2, Zn-H_2 and Zn-CO electrodes have very poor stability. According to these comparative experimental results, the Zn-CO_2 electrode exhibits excellent stability.

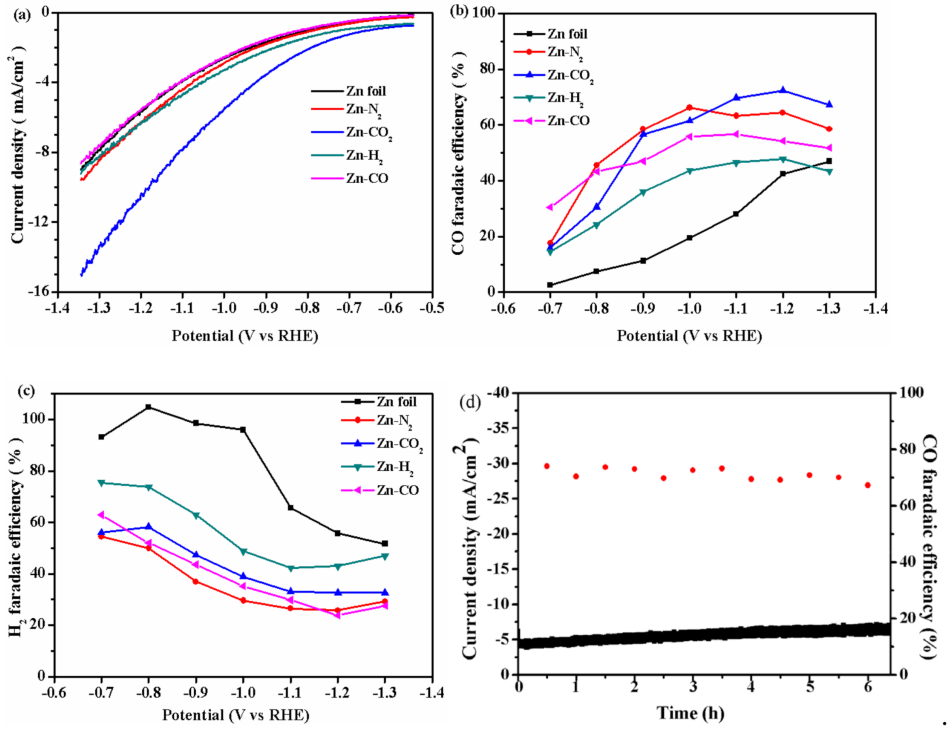

Figure 1. (**a**) Linear sweep voltammetry (**b**) faradaic efficiency (FE) of CO (**c**) FE of H_2 for Zn foil, Zn-N_2, Zn-CO_2, Zn-H_2, Zn-CO electrode at 5 mV/s. (**d**) Current density and FE_{CO} for Zn-CO_2 electrode during 6 h of long-time operation at −1.2 V vs. RHE.

2.2. Characterization of Catalysts

A lot of characterizations were performed to analyze the physical and chemical properties of the catalysts. First of all, XRD was measured to analyze the crystal structure of electrodeposited Zn. Figure 2a exhibits the XRD patterns of all prepared Zn electrodes and Zn foil electrode. It shows that there appear peaks at 36.3°, 39.0°, 43.2°, 54.3°, 70.1°, 70.6°, and 77.0° corresponding to (002), (100), (101), (102), (103), (110) and (004) lattice planes of metallic Zn [JCPDS file No. 04-0831], respectively [28] indicating that Zn catalysts with high crystallinity can be prepared by electrodeposition in different gas-saturated $Zn(NO_3)_2$ aqueous solutions. In order to research the influence of different atmospheres for electrodeposited Zn catalysts, the texture coefficient of each crystal face for the Zn catalysts is calculated and dotted in Figure 2d. The texture coefficients of the Zn (101) plane are 16.79%, 19.16%, 20.79%, 20.6%, 17.59% corresponding to Zn

foil, Zn-N_2, Zn-CO_2, Zn-H_2, Zn-CO electrode, respectively, which are consistent with the trend of corresponding current densities. The Zn-CO_2 electrode has the highest Zn (101) plane ratio while Zn foil has the minimum Zn (101) plane ratio. This is due to the strong binding ability of intermediates formed during $Zn(NO_3)_2$ electroreduction in CO_2-saturated aqueous solutions, which promotes the specific growth of Zn crystals on electrode [26]. As reported in literature [29,30], the Zn (101) plane is conducive to the CO_2RR to CO. On the other hand, the Zn (002) plane is responsible for H_2 evolution in electrochemical CO_2RR [29,30]. The texture coefficients of the Zn (002) plane are 16.00%, 13.16%, 10.51%, 11.27%, 11.85% corresponding to Zn foil, Zn-N_2, Zn-CO_2, Zn-H_2, Zn-CO electrode, respectively. The Zn-CO_2 electrode has a small Zn (002) plane ratio while the Zn foil electrode has the biggest Zn (002) plane ratio. The different proportion of crystal face of Zn catalysts may promote the formation of different morphologies. The greater proportion of Zn (101) promotes the generation of CO on Zn-CO_2 electrode.

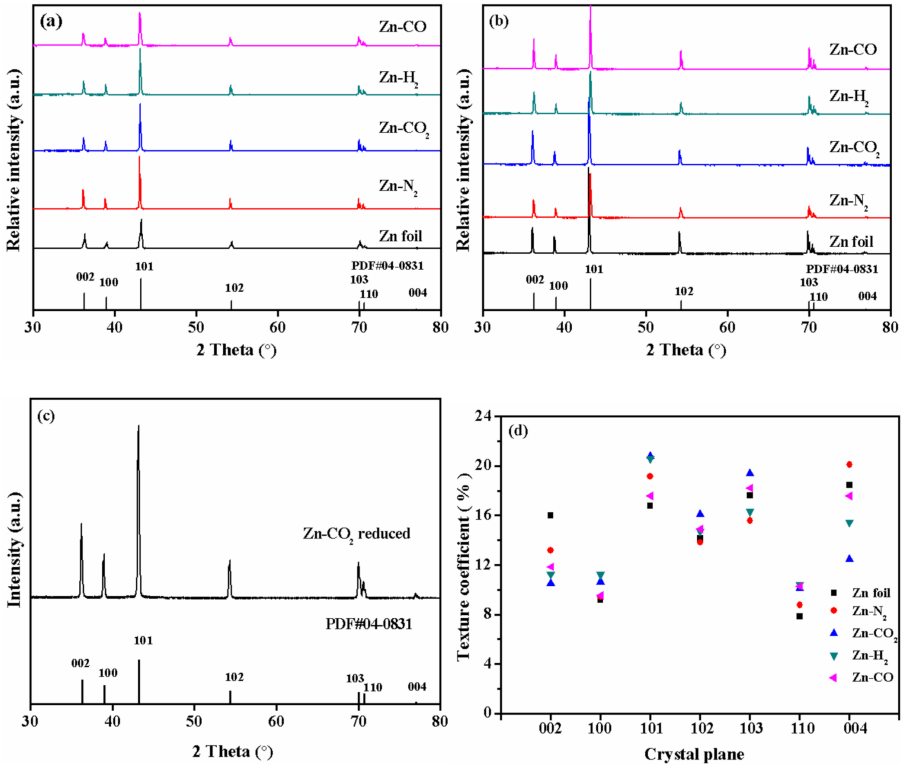

Figure 2. X-ray diffraction (XRD) patterns of prepared Zn electrodes: (**a**) before reaction, (**b**) after reaction and (**c**) the reduced Zn-CO_2 electrode; (**d**) texture coefficients of Zn electrodes before reaction.

The XRD patterns of used catalysts and reduced Zn-CO_2 electrode were also given. As shown in Figure 2b, the XRD patterns of used catalysts are the same as the corresponding fresh catalysts, and there are no any new phases appearing in these catalysts. In the reduced Zn-CO_2 electrode, the XRD pattern also exhibits the characteristic reflections of a single crystalline Zn phase. This indicates that catalyst has been reduced by electrochemical reduction methods.

The surface morphology of representative Zn electrodes was characterized by a scanning electron microscope (SEM) and shown in Figure 3. Obviously, each electrode surface is coarse and porous. On the surface of the Zn-N_2 and Zn-CO electrode, the pore channels with various sizes are found to be partially covered by non-porous sheets. For the Zn-H_2 electrode, these non-porous sheets covered on the surface of the hierarchical pores fully disappear and are replaced by abundant tiny pores. In particular, the surface of the Zn-CO_2 electrode is covered by porous fibers with uniform tiny pores. The different surface morphology should be due to different gas dissolving capacity in $Zn(NO_3)_2$ solution and interaction among gas,

$Zn(NO_3)_2$ and Zn foil. The special morphology of the Zn-CO_2 electrode is just due to the higher solubility of CO_2 in aqueous solution (see Table S2) and a stronger interaction between CO_2 and Zn interface than those of other gases resulting in the stable and uniform growth of Zn crystal during the whole electrodeposition process. Correspondingly, the heterogeneous surface morphology for other electrodes should be related to the low solubility and quick escape of gases from the solution. The surface morphology plays an important role in the CO_2RR on a three-phase interface. According to the relative high current density of CO_2 conversion on the Zn-CO_2 electrode shown in Figure 1a, it can be confirmed that the uniform and abundant tiny pores on the Zn-CO_2 electrode may be more beneficial for CO_2 enrichment by enhancing surface area than other electrodes with low surface area resulting from the bigger pore channels and even non-porous surface. As for the CO and H_2 selectivity, it should be the result of the combined effects, including the pore diffusion and surface enrichment of CO_2 and H_2O molecules, under efficient three-phase contact of CO_2 gas, liquid H_2O and solid catalyst [31]. The high FE_{CO} for the Zn-CO_2 electrode should be attributed to the special surface morphology, which can increase surface area to accommodate high concentrations of CO_2 and the uniform tiny pores on porous fibers are beneficial to CO_2 permeation and detrimental to H_2O molecular diffusion. Instead, the appearance of big pores and non-porous sheets means the shrinkage of surface area, which results in the decrease of surface concentrations of CO_2 and H_2O, but is conducive to the H_2O molecular diffusion, resulting in the possible increase of FE_{H2} and decrease of FE_{CO} in a certain degree. Certainly, the catalytic performance should be determined by the competition between two reactions of CO_2RR to CO and HER (also known as electrochemical water reduction to H_2), which depends on the concentration and diffusion ability of CO_2 and H_2O molecules.

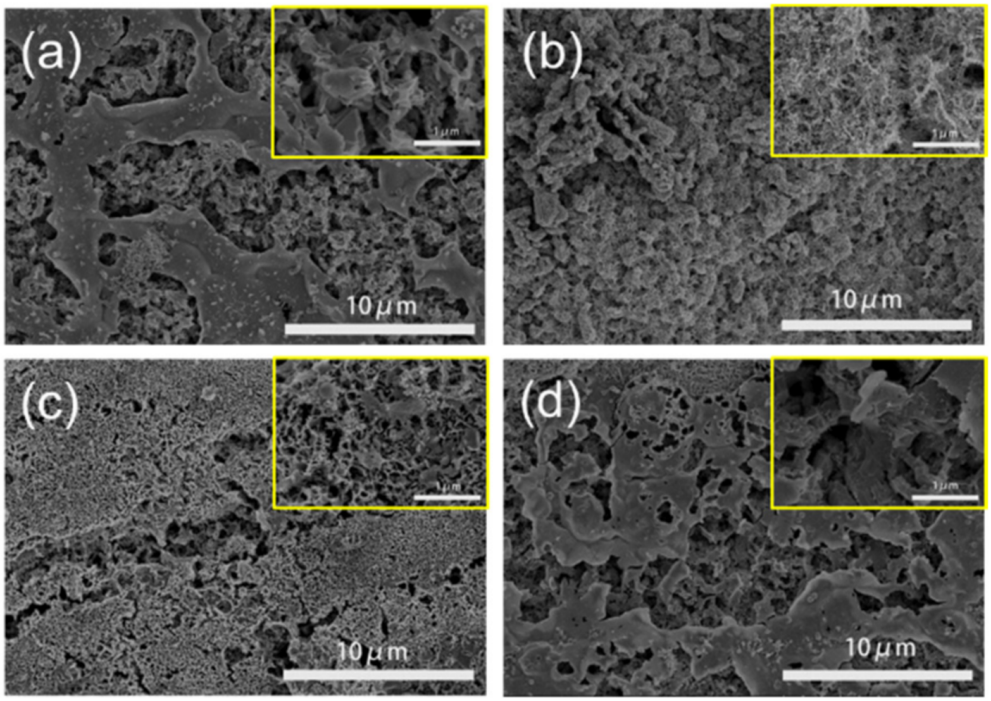

Figure 3. Scanning electron microscope (SEM) images of representative Zn electrodes: (**a**) Zn-N_2, (**b**) Zn-CO_2, (**c**) Zn-H_2, (**d**) Zn-CO.

In addition, we compared the morphology of the catalyst after the reaction (Figure 4) and found that the Zn foil, Zn-N_2 and Zn-CO_2 catalysts accumulated into a regular nanosheet structure. The nanosheet of the Zn-N_2 electrode is much larger in size than other electrodes after reaction, and more irregular than other electrodes. It is the reason that current density is higher in the initial stage and more unstable. The nanosheet greatly reduced the ECSA of the catalysts, which was one of the reasons for the catalyst's death, after 6 h of reaction.

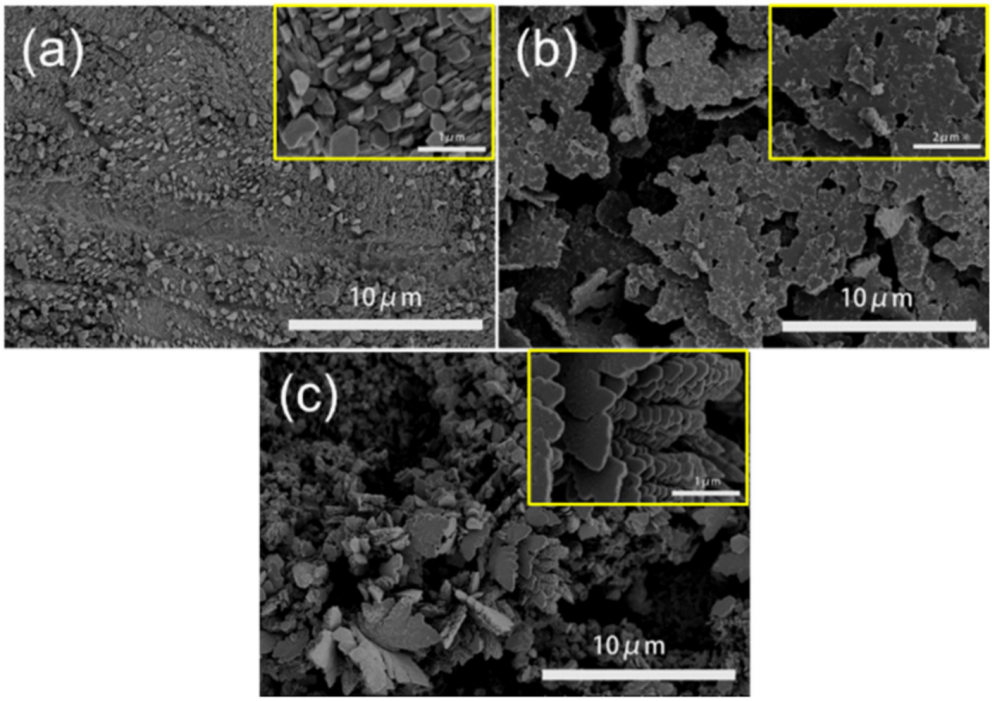

Figure 4. SEM images of representative Zn electrodes after reaction: (**a**) Zn foil electrode, (**b**) Zn-N_2 electrode, (**c**) Zn-CO_2 electrode.

Furthermore, the representative Zn-N_2 and Zn-CO_2 electrodes were also analyzed by transmission electron microscope (TEM) and the TEM images for these representative samples are shown in Figure 5. The nanosheets can be found easily on each sample, which constructs the skeleton of pore channels. Obviously, the size of nanosheets on the Zn-CO_2 electrode is uniform and far less than that on the Zn-N_2 electrode. The results are consistent with those of SEM. In addition, the existence of the Zn (002) plane can further be demonstrated by the lattice spacing of 0.24 nm of two electrodes. Besides the metal Zn phase, the characteristic spacing of 0.26 nm for ZnO (002) for the Zn-N_2 electrode, and 0.28 nm for the ZnO (100) lattice plane for the Zn-CO_2 electrode can be seen. The results also confirm that ZnO can be formed during the preparation process, indicating the importance of electrochemical reduction of the electrode prior to the reaction.

X-ray photoelectron spectroscopy (XPS) was performed to demonstrate the chemical states of Zn and O elements on the surface of the catalysts. The XPS spectra are given in Figure 6 and the characteristics data are collected in Table 1. According to the XPS survey scan as shown in Figure 6a, it can be further confirmed that Zn and O elements exist on the Zn-N_2 and Zn-CO_2 electrodes. As for the XPS spectra of Zn 2P region, there are two deconvoluted peaks (Figure 6b). The peak at 1021.8 eV is associated with Zn $2P_{3/2}$. Figure 6c shows the Zn $2P_{3/2}$ spectrum of Zn-N_2 and Zn-CO_2 electrode. It shows Zn in two states, 1021.5 eV and 1022.1 eV, respectively. The low binding energy (BE) peak can be assigned to the metallic Zn (Zn^0), while the high BE peak should be ascribed to the oxidized Zn (Zn^{2+}). The ratio of Zn^{2+}/total of Zn-CO_2 electrode is higher than that of the Zn-N_2 electrode, it is due to the fibrous structure and pore diameter resulting in the formation of more under-coordinated Zn^{2+} species on the surface of small particles, especially at the tip of pore mouths [25]. Before the reaction, the reduction treatment can transfer the under-coordinated Zn^{2+} species into active Zn species. These oxidized Zn sites may facilitate the adsorption of reactants and *COOH intermediates on the surface of the Zn electrode, thus improving the generation of CO in the reaction [32]. Moreover, three fitted peaks can be seen in the O 1s regions. The peak at 530.6 eV is associated with O^{2-} from ZnO. The peak at 531.8 eV is related to hydroxyl group on the surface [33] and the peak at 532.8 eV is attributed to adsorbed oxygen. The adsorbed oxygen comes from oxygen in the absorbed water molecules [32,34]. The proportion of O 1s peak at

530.6 eV, associated with ZnO in the Zn-CO_2 electrode, is higher than the Zn-N_2 electrode. It indicated that the presence of CO_2 will promote the formation of under-coordinated Zn^{2+} species on the surface of the Zn electrode in the process of electrodeposition. The under-coordinated Zn^{2+} may facilitates the adsorption of *COOH intermediates on the surface of the Zn electrode and enhances the ability of intermediate to bind with the Zn electrode [35]. But this is not the significant distraction factor for catalytic excellent performance of Zn-CO_2. It is because Zn-N_2 and Zn-CO_2 electrodes have the under-coordinated Zn^{2+} and the difference between them is not particularly great.

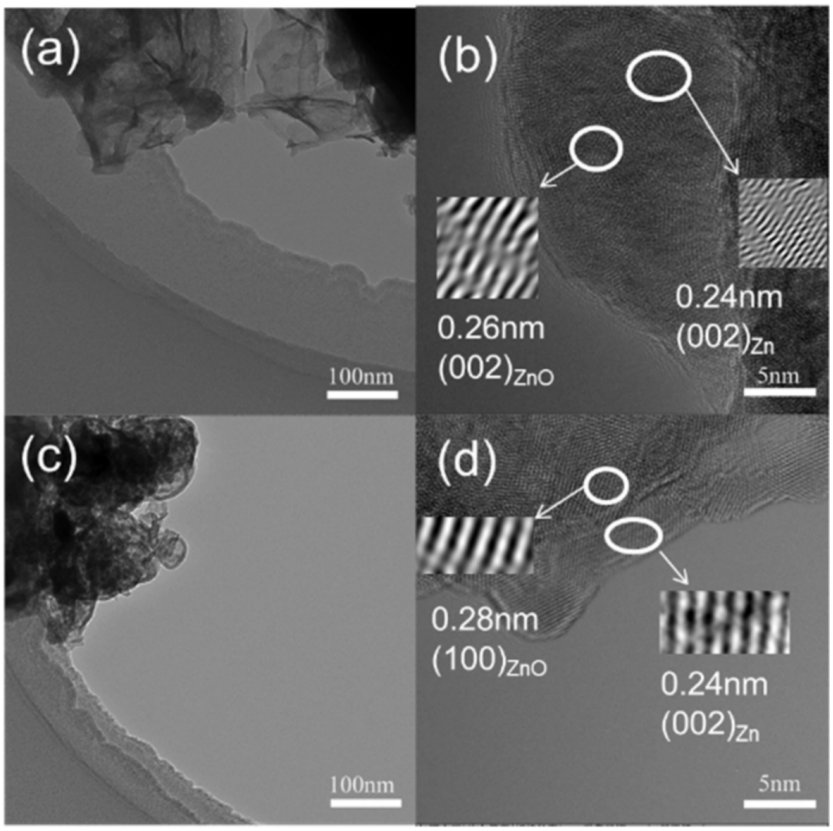

Figure 5. Transmission electron microscopy (TEM) images of (**a**,**b**) Zn-N_2 electrode and (**c**,**d**) Zn-CO_2 electrode.

In order to explore the reasons for the superior CO_2RR performance of Zn-CO_2 electrode, it is necessary to compare the ECSA of each electrode by measuring their specific double-layer capacitance calculated by a CV scan in Figure S2. The result is shown in Figure S2, and the data of specific double-layer capacitance were calculated from this result. The line regression of the double layer capacitance and Tafel plot are displayed in Figure 7 and the corresponding ECSA and Tafel slope data of all samples are summarized in Table 2. The results show that the Zn-CO_2 electrode has the largest ECSA value (19.295 mF/cm^2) which is 60 times that of the Zn foil electrode (0.309 mF/cm^2), and the other electrodes, Zn-N_2, Zn-H_2 and Zn-CO, give a lower ECSA value (from 2.210 to 4.835 mF/cm^2). The quite high ECSA for Zn-CO_2 electrode is related to the special porous fibers with uniform tiny pores, which can enhance the surface concentration and diffusion ability of CO_2. In general, during electrodeposition, the presence of CO_2 affects the growth of crystal surfaces and promotes the formation of porous fibers morphology, which leads to a larger ECSA. This is the main reason for excellent performance of electrochemical CO_2RR for the Zn-CO_2 electrode.

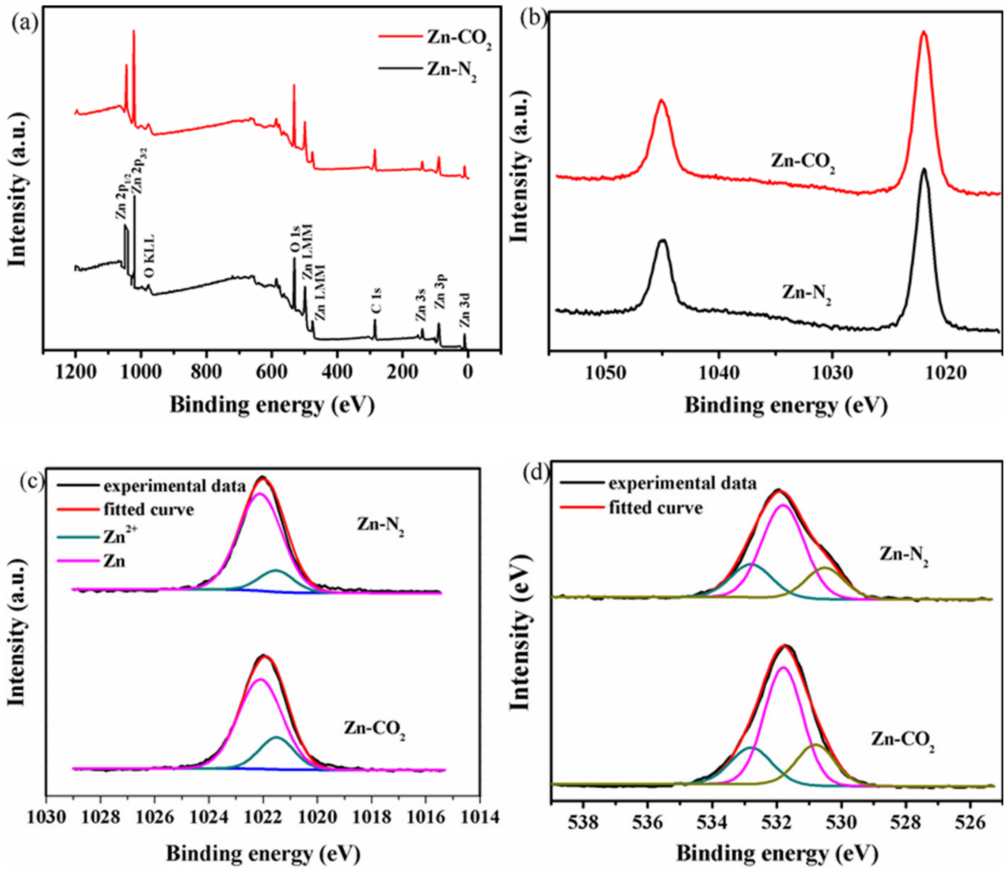

Figure 6. XPS spectra of (**a**) overall survey scan, (**b**) Zn 2P, (**c**) Zn $2P_{3/2}$, (**d**) O 1s for the Zn-N_2 and Zn-CO_2 electrodes.

Table 1. X-ray photoelectron spectroscopy (XPS) characteristics data of Zn $2P_{3/2}$ and O 1s regions for the Zn-N_2 and Zn-CO_2 electrodes.

Catalysts	Binding Energy (eV)		Peak Area Ratio [a]	Binding Energy (eV)			Peak Area Ratio
	Zn^{2+}	Zn^0	Zn^{2+}/Total	Oa	Ob	Oc	O/Total
Zn-N_2	1021.5	1022.1	0.15	532.8	531.8	530.6	0.21:0.61:0.18
Zn-CO_2	1021.5	1022.1	0.22	532.8	531.7	530.7	0.20:0.59:0.21

[a] Calculated from the fitting peak area results of Zn $2P_{3/2}$ and O 1s XPS spectra.

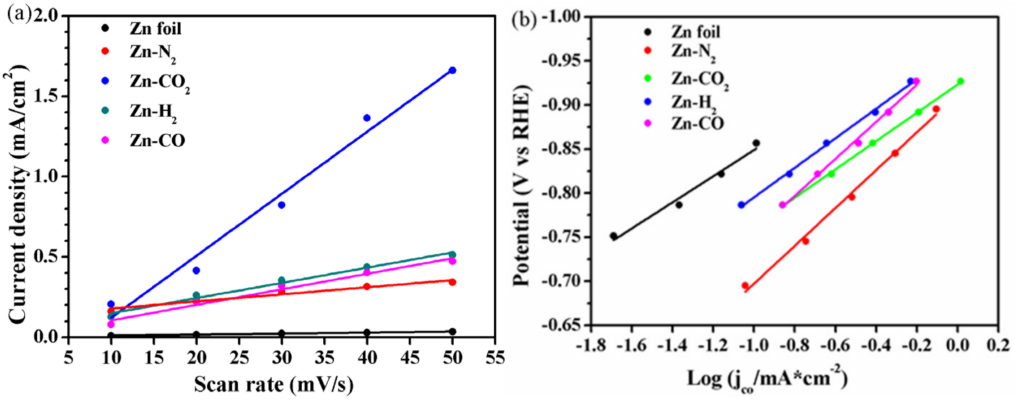

Figure 7. (**a**) The line regression of the double layer capacitance and (**b**) Tafel Plot for CO_2RR over Zn foil, Zn-N_2, Zn-CO_2, Zn-H_2, Zn-CO electrode in CO_2-saturated 0.1M $KHCO_3$ electrolyte.

Table 2. The electrochemical active surface area (ECSA) and Tafel slope data of all samples.

Sample	ECSA (mF/cm^2)	Tafel Slope (mV/dec)
Zn foil	0.309	211.70
Zn-N_2	2.210	214.80
Zn-CO_2	19.295	229.34
Zn-H_2	4.735	239.54
Zn-CO	4.835	253.28

To elucidate the origin of the remarkable CO_2RR performance over our catalysts, we performed detailed electrokinetic studies to compare the CO_2 reduction pathway on all electrodes by comparing the experimentally observed Tafel slope (logarithm of the partial current density towards a specific product vs. potential). There are four elementary reaction steps for CO_2RR to CO:

$$*CO_2 + e^- \rightarrow *CO_2^- \quad (1)$$

$$*CO_2^- + H^+ \rightarrow *COOH \quad (2)$$

$$*COOH + H^+ + e^- \rightarrow *CO + H_2O\ (l) \quad (3)$$

$$*CO \rightarrow CO + * \quad (4)$$

where * represents an active site. Firstly, the absorbed CO_2 gains an electron to form to $*CO_2^-$ anion radical. Secondly, the $*CO_2^-$ anion radical binds with a proton to form the *COOH intermediate. Thirdly, the *COOH intermediate gains a proton and an electron and is reduced *CO intermediated and H_2O. Finally, the *CO is desorbed from the surface of catalysts to form CO. It is well known that the value of a Tafel slope can reflect the rate-control steps of the reaction under certain conditions. Figure 7b shows that Zn-CO_2 electrode and Zn foil have Tafel slope of 229.34 mV/dec and 211.7 mV/dec, respectively. These are close to the theoretical value of 250 mV/dec for a rate limiting step at higher overpotential (−0.6 to −0.7 V) [24,36]. The higher value implies that the initial electron transfer step is the rate-determining step (RDS) [28]. The Zn-H_2 and Zn-CO electrodes have higher Tafel slope of 239.54 mV/dec and 253.28 mV/dec. From these data, it can be inferred that the RDS of electrochemical reduction reaction is mainly the first step of electron transfer step on these Zn electrodes. This indicated the $*CO_2^-$ intermediate plays a crucial role in the CO_2RR reaction. The same RDS indicated that the CO_2RR reaction may have similar intrinsic activity on these Zn catalysts [24].

3. Experimental Section

3.1. Fabrication of Zn Catalysts

Zn foil electrodes (1 cm × 2 cm) were prepared by mechanical polishing using sandpaper (800 grit), followed by sonication in acetone, ethanol and deionized water for 30 min. $Zn(NO_3)_2$ (Tianjin Fengchen Chemical Regents Factory, Tianjin, China)aqueous solution (30 mL, 0.05 M) was purged with different gases (N_2, CO_2, H_2, CO) as a precursor solution. A chronoamperometry experiment setting at −1.85 V vs. SCE (300 s) was used to reduce Zn precursor to metallic Zn on the surface of the prepared Zn foil electrode. After deposition, the electrode was rinsed by deionized water and then immediately taken for electrochemical testing to prevent electrode oxidation again.

3.2. Eelectrocatalytic Test for CO_2RR

An electrochemical workstation (CHI instrument 660E, Chenhua, Shanghai, China) was used for all electrochemical tests. The electrochemical measurements were performed in a three-electrode system. The reference electrode was a saturated calomel electrode (SCE)

and the counter electrode was a Pt sheet, respectively. All potentials in this work are quoted versus the reversible hydrogen electrode (RHE), according to the Nernst equation of:

$$E_{RHE} = E_{SCE} + 0.0591 * PH + 0.241 \quad (5)$$

CO_2RR was conducted in a gas-tight two component H-type electrochemical cell separated by Nafion 117 cation-exchange membrane (Dupont, Wilmington, DE, USA). 0.1 M $KHCO_3$ (99.5%) aqueous solution was used as electrolyte and was purged with CO_2 (99.999%) at a rate of 20 mL/min for at least 30 min before the testing of CO_2RR. During the testing, the electrolyte was stirred by a magnetic stirring apparatus. The gas phase products were detected by a gas chromatograph (GC, SP2100) which was equipped with a TDX-01 column. A flame ionization detector (FID) was equipped with methanizer to analyze CO and a thermal conductivity detector (TCD) to analyze H_2. The FE of product was calculated by Equation (6).

$$\text{FE\%} = \frac{znF}{Q} \times 100\% \quad (6)$$

where z is 2 for CO_2RR to CO or H_2, n is the mole number of the products, Faraday's constant F is 96,485 C/mol, and Q is the total charge passed.

3.3. Catalyst Characterization

XRD tests were performed on a D8-Foucas (BRUKER AXS GMBH, Karlsruhe, Germany) equipped with a Cu Kα radiation (λ = 0.15418 nm). The spectra were collected between 2θ ranges of 30–80°, at a scanning speed of 8°/min.

To compare the crystal facet ratio of different Zn catalysts, texture coefficients [29] were calculated by Equation (7).

$$TC_{hkl} = \frac{I_{(hkl)}/I_{0(hkl)}}{\sum_{i=1}^{n} I_{(hkl)}/I_{0(hkl)}} \times 100\% \quad (7)$$

where $I_{(hkl)}$ is the diffraction intensity of the (*hkl*) facet and is automatically calculated by the Jade software, $I_{0(hkl)}$ is the standard diffraction intensity of the *(hkl)* and taken from JCPDS#04-0831, and n is the number of diffraction peaks of Zn (n = 7).

The TEM images of Zn catalysts were tested by a JEM2100-F field-emission transmission electron microscope (JEOL, Tokyo, Japan). The field SEM images of Zn catalysts were tested by a Regulus 8100 instrument (JEOL, Tokyo, Japan) at a 3.0 KV electron beam. The surface chemical states of the Zn electrode were investigated by XPS (ULVACPHI, Japan) with monochromatized Al Kα X-ray radiation (1486.6 eV).

4. Conclusions

In summary, a series of Zn catalysts were prepared by electrodeposition in different gas conditions (N_2, CO_2, H_2, CO). The Zn-CO_2 catalyst obtained with porous fibers and uniform tiny pores exhibited high activity and selectivity for CO_2RR to CO, with FE_{CO} for 73.0% and FE_{H2} for 32.6% at −1.2 V vs. RHE. The partial current density of CO was 6.14 mA/cm^2 and the FE_{CO} was almost unchanged over 6 h in −1.2 V vs. RHE. The electrokinetic study results show that the initial electron transfer step was the RDS for the Zn-CO_2 electrode. The presence of CO_2 affected the crystal growth of electrodeposited Zn, increased the proportion of the Zn (101) crystal on the Zn electrode surface, and induced the formation of a fibrous and porous structure. The structure increased the ECSA and under-coordinated Zn^{2+} species. The greater ECSA provided more active sites and promoted the production of CO. This was the main reason for the excellent performance of electrochemical CO_2RR for the Zn-CO_2 electrode. This study demonstrates that the morphology and crystal structure of Zn catalysts have a great influence on the activity for

CO_2RR. This work is of great value and significance to solve the challenge of low activity and poor stability in electrochemical CO_2RR.

Supplementary Materials: The following are available online at https://www.mdpi.com/article/10.3390/catal11040477/s1, Figure S1: Current density and FE_{CO} for (a) Zn foil, (b) Zn-N_2, (c) Zn-H_2 and (d) Zn-CO electrodes during 6 h of long-time operation at −1.2 V vs. RHE; Figure S2: CV curves on (a) Zn foil, (b) Zn-N_2, (c) Zn-CO_2, (d) Zn-H_2 and (e) Zn-CO electrodes with a potential range from −0.415 to −0.515 V vs. RHE in a N_2 bubbled 1 M Na_2SO_4 electrolyte; Table S1: The data of CO partial current density for Zn-CO_2 electrode; Table S2: The solubility data of different gases in water.

Author Contributions: M.G. wrote the manuscript, performed the experiments and analyzed data; M.G., X.L. and Y.H. collected references and characterized the physic-chemical properties of materials; L.L. and J.L. collected and checked data; Y.X. and Y.L. analyzed data and checked the manuscript; L.Z. provided research ideas, analyzed data and revised the manuscript. All authors have read and agreed to the published version of the manuscript.

Funding: This research was funded by National Natural Science Foundation of China (21776214) and Natural Science Foundation of Jiangsu Province (BK20161166).

Data Availability Statement: Data is contained within the article or Supplementary.

Conflicts of Interest: The authors declare no conflict of interest.

References

1. Zheng, T.; Jiang, K.; Ta, N.; Hu, Y.; Zeng, J.; Liu, J.; Wang, H. Large-scale and highly selective CO_2 electrocatalytic reduction on nickel single-atom catalyst. *Joule* **2019**, *3*, 265–278. [CrossRef]
2. Kim, S.; Dong, W.J.; Gim, S.; Sohn, W.; Park, J.Y.; Yoo, C.J.; Jang, H.W.; Lee, J.-L. Shape-controlled bismuth nanoflakes as highly selective catalysts for electrochemical carbon dioxide reduction to formate. *Nano Energy* **2017**, *39*, 44–52. [CrossRef]
3. Kas, R.; Kortlever, R.; Milbrat, A.; Koper, M.T.; Mul, G.; Baltrusaitis, J. Electrochemical CO_2 reduction on Cu_2O-derived copper nanoparticles: Controlling the catalytic selectivity of hydrocarbons. *Phys. Chem. Chem. Phys.* **2014**, *16*, 12194–12201. [CrossRef] [PubMed]
4. Albo, J.; Irabien, A. Cu_2O-loaded gas diffusion electrodes for the continuous electrochemical reduction of CO_2 to methanol. *J. Catal.* **2016**, *343*, 232–239. [CrossRef]
5. Sarfraz, S.; Garcia-Esparza, A.T.; Jedidi, A.; Cavallo, L.; Takanabe, K. Cu–Sn bimetallic catalyst for selective aqueous electroreduction of CO_2 to CO. *ACS Catal.* **2016**, *6*, 2842–2851. [CrossRef]
6. Lamaison, S.; Wakerley, D.; Montero, D.; Rousse, G.; Taverna, D.; Giaume, D.; Mercier, D.; Blanchard, J.; Tran, H.N.; Fontecave, M.; et al. Zn-Cu alloy nanofoams as efficient catalysts for the reduction of CO_2 to syngas mixtures with a potential-independent H_2/CO ratio. *ChemSusChem* **2019**, *12*, 511–517. [CrossRef]
7. Fan, Q.; Zhang, M.; Jia, M.; Liu, S.; Qiu, J.; Sun, Z. Electrochemical CO_2 reduction to C^{2+} species: Heterogeneous electrocatalysts, reaction pathways, and optimization strategies. *Mater. Today Energy* **2018**, *10*, 280–301. [CrossRef]
8. Francis, S.A.; Velazquez, J.M.; Ferrer, I.M.; Torelli, D.A.; Guevarra, D.; McDowell, M.T.; Sun, K.; Zhou, X.; Saadi, F.H.; John, J.; et al. Reduction of aqueous CO_2 to 1-propanol at MoS_2 electrodes. *Chem. Mater.* **2018**, *30*, 4902–4908. [CrossRef]
9. Zhu, W.; Michalsky, R.; Metin, O.; Lv, H.; Guo, S.; Wright, C.J.; Sun, X.; Peterson, A.A.; Sun, S. Monodisperse au nanoparticles for selective electrocatalytic reduction of CO_2 to CO. *J. Am. Chem. Soc.* **2013**, *135*, 16833–16836. [CrossRef]
10. Kim, J.-H.; Youn, D.H. Nanostructured sponge-like au for selective electrochemical reduction of carbon dioxide. *Chem. Phys. Lett.* **2018**, *704*, 27–30. [CrossRef]
11. Chen, Y.; Li, C.W.; Kanan, M.W. Aqueous CO_2 reduction at very low overpotential on oxide-derived Au nanoparticles. *J. Am. Chem. Soc.* **2012**, *134*, 19969–19972. [CrossRef]
12. Fang, Y.X.; Flake, J.C. Electrochemical reduction of CO_2 at functionalized Au electrodes. *J. Am. Chem. Soc.* **2017**, *139*, 3399–3405. [CrossRef]
13. Lee, H.; Kim, S.K.; Ahn, S.H. Electrochemical preparation of Ag/Cu and Au/Cu foams for electrochemical conversion of CO_2 to CO. *J. Ind. Eng. Chem.* **2017**, *54*, 218–225. [CrossRef]
14. Sastre, F.; Muñoz-Batista, M.J.; Kubacka, A.; Fernández-García, M.; Smith, W.A.; Kapteijn, F.; Makkee, M.; Gascon, J. Efficient electrochemical production of syngas from CO_2 and H_2O by using a nanostructured Ag/g-C_3N_4 catalyst. *ChemElectroChem* **2016**, *3*, 1497–1502. [CrossRef]
15. Ma, M.; Liu, K.; Shen, J.; Kas, R.; Smith, W.A. In situ fabrication and reactivation of highly selective and stable Ag catalysts for electrochemical CO_2 conversion. *ACS Energy Lett.* **2018**, *3*, 1301–1306. [CrossRef]

16. Gao, Y.; Li, F.; Zhou, P.; Wang, Z.; Zheng, Z.; Wang, P.; Liu, Y.; Dai, Y.; Whangbo, M.-H.; Huang, B. Enhanced selectivity and activity for electrocatalytic reduction of CO_2 to CO on an anodized Zn/carbon/Ag electrode. *J. Mater. Chem. A* **2019**, *7*, 16685–16689. [CrossRef]
17. Lamaison, S.; Wakerley, D.; Blanchard, J.; Montero, D.; Rousse, G.; Mercier, D.; Marcus, P.; Taverna, D.; Giaume, D.; Mougel, V.; et al. High-current-density CO_2-to-CO electroreduction on Ag-alloyed Zn dendrites at elevated pressure. *Joule* **2020**, *4*, 395–406. [CrossRef]
18. Singh, M.R.; Goodpaster, J.D.; Weber, A.Z.; Head-Gordon, M.; Bell, A.T. Mechanistic insights into electrochemical reduction of CO_2 over ag using density functional theory and transport models. *Proc. Natl. Acad. Sci. USA* **2017**, *114*, E8812–E8821. [CrossRef]
19. Guo, W.; Shim, K.; Kim, Y.T. Ag layer deposited on Zn by physical vapor deposition with enhanced CO selectivity for electrochemical CO_2 reduction. *Appl. Surf. Sci.* **2020**, 526. [CrossRef]
20. Li, C.; Shen, G.; Zhang, R.; Wu, D.; Zou, C.; Ling, T.; Liu, H.; Dong, C.; Du, X.-W. Zn nanosheets coated with a ZnS subnanometer layer for effective and durable CO_2 reduction. *J. Mater. Chem. A* **2019**, *7*, 1418–1423. [CrossRef]
21. Nguyen, D.L.T.; Jee, M.S.; Won, D.H.; Oh, H.-S.; Min, B.K.; Hwang, Y.J. Effect of halides on nanoporous Zn-based catalysts for highly efficient electroreduction of CO_2 to CO. *Catal. Commun.* **2018**, *114*, 109–113. [CrossRef]
22. Moreno-Garcia, P.; Schlegel, N.; Zanetti, A.; Cedeno Lopez, A.; Galvez-Vazquez, M.J.; Dutta, A.; Rahaman, M.; Broekmann, P. Selective electrochemical reduction of CO_2 to CO on Zn-based foams produced by $Cu^{(2+)}$ and template-assisted electrodeposition. *ACS Appl. Mater. Interfaces* **2018**, *10*, 31355–31365. [CrossRef] [PubMed]
23. Morimoto, M.; Takatsuji, Y.; Hirata, K.; Fukuma, T.; Ohno, T.; Sakakura, T.; Haruyama, T. Visualization of catalytic edge reactivity in electrochemical CO_2 reduction on porous Zn electrode. *Electrochim. Acta* **2018**, *290*, 255–261. [CrossRef]
24. Luo, W.; Zhang, J.; Li, M.; Züttel, A. Boosting co production in electrocatalytic CO_2 reduction on highly porous Zn catalysts. *ACS Catal.* **2019**, *9*, 3783–3791. [CrossRef]
25. Rosen, J.; Hutchings, G.S.; Lu, Q.; Forest, R.V.; Moore, A.; Jiao, F. Electrodeposited Zn dendrites with enhanced CO selectivity for electrocatalytic CO_2 reduction. *ACS Catal.* **2015**, *5*, 4586–4591. [CrossRef]
26. Wang, H.; Liang, Z.; Tang, M.; Chen, G.; Li, Y.; Chen, W.; Lin, D.; Zhang, Z.; Zhou, G.; Li, J.; et al. Self-selective catalyst synthesis for CO_2 reduction. *Joule* **2019**, *3*, 1927–1936. [CrossRef]
27. Wang, Y.; Wang, Z.; Dinh, C.-T.; Li, J.; Ozden, A.; Golam Kibria, M.; Seifitokaldani, A.; Tan, C.-S.; Gabardo, C.M.; Luo, M.; et al. Catalyst synthesis under CO_2 electroreduction favours faceting and promotes renewable fuels electrosynthesis. *Nat. Catal.* **2019**, *3*, 98–106. [CrossRef]
28. Zhang, T.; Li, X.; Qiu, Y.; Su, P.; Xu, W.; Zhong, H.; Zhang, H. Multilayered Zn nanosheets as an electrocatalyst for efficient electrochemical reduction of CO_2. *J. Catal.* **2018**, *357*, 154–162. [CrossRef]
29. Qin, B.; Li, Y.; Fu, H.; Wang, H.; Chen, S.; Liu, Z.; Peng, F. Electrochemical reduction of CO_2 into tunable syngas production by regulating the crystal facets of earth-abundant Zn catalyst. *ACS Appl. Mater. Interfaces* **2018**, *10*, 20530–20539. [CrossRef]
30. Won, D.H.; Shin, H.; Koh, J.; Chung, J.; Lee, H.S.; Kim, H.; Woo, S.I. Highly efficient, selective, and stable CO_2 electroreduction on a hexagonal Zn catalyst. *Angew. Chem. Int. Ed.* **2016**, *55*, 9297–9300. [CrossRef]
31. Li, J.; Chen, G.; Zhu, Y.; Liang, Z.; Pei, A.; Wu, C.-L.; Wang, H.; Lee, H.R.; Liu, K.; Chu, S.; et al. Efficient electrocatalytic CO_2 reduction on a three-phase interface. *Nat. Catal.* **2018**, *1*, 592–600. [CrossRef]
32. Nguyen, D.L.T.; Jee, M.S.; Won, D.H.; Jung, H.; Oh, H.-S.; Min, B.K.; Hwang, Y.J. Selective CO_2 reduction on zinc electrocatalyst: The effect of zinc oxidation state induced by pretreatment environment. *ACS Sustain. Chem. Eng.* **2017**, *5*, 11377–11386. [CrossRef]
33. Kim, W.G.; Tak, Y.J.; Du Ahn, B.; Jung, T.S.; Chung, K.B.; Kim, H.J. High-pressure gas activation for amorphous indium-gallium-zinc-oxide thin-film transistors at 100 degrees c. *Sci. Rep.* **2016**, *6*, 23039. [CrossRef]
34. Hong, Y.; Tian, C.; Jiang, B.; Wu, A.; Zhang, Q.; Tian, G.; Fu, H. Facile synthesis of sheet-like ZnO assembly composed of small ZnO particles for highly efficient photocatalysis. *J. Mater. Chem. A* **2013**, 1. [CrossRef]
35. Geng, Z.; Kong, X.; Chen, W.; Su, H.; Liu, Y.; Cai, F.; Wang, G.; Zeng, J. Oxygen vacancies in ZnO nanosheets enhance CO_2 electrochemical reduction to CO. *Angew. Chem. Int. Ed.* **2018**, *57*, 6054–6059. [CrossRef]
36. Dunwell, M.; Luc, W.; Yan, Y.; Jiao, F.; Xu, B. Understanding surface-mediated electrochemical reactions: CO_2 reduction and beyond. *ACS Catal.* **2018**, *8*, 8121–8129. [CrossRef]